Title: **Autonomous Microstructure EM-APEX Floats**

Authors: Ren-Chieh Lien[1,2], Thomas B. Sanford[1,2], James A. Carlson[1], and John H. Dunlap[1]
[1] Applied Physics Laboratory, University of Washington, Seattle, WA
[2] School of Oceanography, University of Washington, Seattle, WA

Corresponding author:
Ren-Chieh Lien
Applied Physics Laboratory, University of Washington
1013 NE 40th Street
Seattle, WA 98105
rcl@uw.edu

Abstract:

Fast responding FP-07 thermistors have been incorporated on profiling EM-APEX floats to measure microscale ocean temperature fluctuations produced by turbulence. In this implementation, the FP-07 thermistor generates an electrical signal corresponding to ocean temperature fluctuations, which is conditioned by an analog circuit board, and digitized and recorded to a custom data acquisition and storage board. The raw and processed temperature observations are stored on a microSD card. Results from eight microstructure EM-APEX floats deployed in the Sargasso Sea are presented here. The slow profiling speed of EM-APEX floats enables them to capture the higher wavenumber regime of microscale temperature variation. The quality of temperature variance dissipation rates χ estimated from microstructure EM-APEX floats is verified by their agreement with the Batchelor spectrum and by the close inter-float agreement of temporal and vertical variations measured by multiple floats. Estimates of χ from the profiling floats exhibit a lognormal distribution as expected for statistically homogeneous isotropic turbulence. Turbulence measurements derived from FP-07 sensors on autonomous profiling floats are of comparable quality to those on conventional free-fall microstructure profilers.

1. Introduction

Quantifying oceanic turbulence, diffusion, and dissipation gives insight to important oceanic processes and improves parameterization schemes in numerical models. The intermittency of turbulence and the difficulty obtaining adequate realizations of turbulence observations limit the reliability of turbulence estimations. One sensor, the FP-07 thermistor, is capable of rapid temperature sampling at microscales, and has been used extensively on free-fall vertical profilers and moorings (*Gregg and Meagher*, 1980; *Moum and Nash*, 2009). The temperature variance dissipation rate χ can be computed from FP-07 microscale temperature measurements. The development of autonomous vertical profilers and the ability to deploy several in an array allows collection of many profiles at multiple sites simultaneously. Because of the dynamical link between turbulence and small-scale vertical shear and strain, autonomous profiling floats with FP-07 thermistors as well as other sensors to observe conventional water properties are ideal to better measure and understand small-scale and microscale processes and improve physics-based turbulence parameterization schemes. Here, we describe our approach to implement turbulence sensing on the EM-APEX float and present results from deployments of multiple floats.

2. Material and methods

2.1 EM-APEX floats

The EM-APEX float combines the standard Teledyne Webb Research Corp. APEX profiling float with an APL-UW subsystem that measures the motion-induced electric fields generated by the ocean currents moving through the vertical component of the earth's magnetic field (Fig. 1) (*Sanford et al*., 2005). The APEX float changes its buoyancy to enable it to profile the ocean with a maximum depth range of 2000 m. Temperature and salinity measurements are obtained from a Sea-Bird Electronics SBE41CP CTD, and taken every 10–25 s. When on the sea surface, the float's position is determined by GPS, and the position and accumulated profile data (except for the raw FP-07 data) are transmitted over the Iridium global satellite phone system.

The velocity sensor operates on the same principles of motional induction applied on the Absolute Velocity Profiler (*Sanford et al*., 1985) and the Expendable Current Profiler (*Sanford et al*., 1982). The electric field sensing electrodes are located on the top end of the floats. Other necessary measurements are magnetic compass heading and instrument tilt. The float descends and ascends at ~0.15 m s^{-1} and rotates at a period of ~12 s. The motional-induced electric field is determined by a sinusoidal fit to the measured voltages using the basis functions from the horizontal components of the magnetometer. The fit is made over a 50-s-long segment of data, and the averaging window is moved 25 s between successive fits. These sinusoidal fits and the rms (root mean square) residuals are transferred to the APEX float controller for storage and later transmission over Iridium. The fits provide an estimate of the horizontal current, and the rms residuals provide an estimate of the velocity noise level. In the upper ocean, the rms residuals can also be used to estimate properties of surface gravity waves, e.g., amplitude, period, and wavelength. The horizontal current uncertainty is about 0.015 m s^{-1}.

2.2 Turbulence sensor implementation

A fast-response temperature sensor, the FP-07 thermistor, and electronic signal conditioning board are provided by Rockland Scientific, Inc. (RSI), and combined with a custom digital data

acquisition board. The complete unit is installed in EM-APEX floats (Fig. 1). In addition to the thermistors installed in metal shafts or stings, the implementation requires special end caps for the EM-APEX float.

The arrangement of the major components within the EM-APEX float is outlined in a block diagram (Fig. 2). Temperature fluctuations cause the FP-07 thermistor to change its resistance. Electric current passing through the FP-07 thermistor produces voltage fluctuations caused by these resistance fluctuations. The voltages are amplified and conditioned on the RSI μASTP-LP board and passed to the APL-UW board. The APL-UW board (MLADC) digitizes the amplified voltage signals to 24-bit resolution. The board also contains a low-power microprocessor that buffers and stores the digital data onto a microSD card. In the latest version of the microstructure package, temperature spectra are computed and band-averaged spectra are transmitted over Iridium. The turbulence circuitry is powered and controlled by the APEX controller APF-9 board.

2.3 Estimates of χ, turbulent temperature diffusivity K_T, and turbulent kinetic energy dissipation rate ε

The high-frequency FP-07 sensor provides measurements of turbulent temperature fluctuations that can be used to compute the temperature variance dissipation rate χ, turbulent temperature diffusivity K_T, and turbulent kinetic energy dissipation rate ε. The temperature variance dissipation rate for isotropic turbulence is defined as

$$\chi = 2D_T \left\langle \left(\frac{\partial T}{\partial x}\right)^2 + \left(\frac{\partial T}{\partial y}\right)^2 + \left(\frac{\partial T}{\partial z}\right)^2 \right\rangle = 6\, D_T \left\langle \left(\frac{\partial T}{\partial z}\right)^2 \right\rangle = 6\, D_T \int_{k_o}^{\infty} \phi_{\partial_z T}(k_z) dk_z$$

where D_T is the molecular temperature diffusivity (~1.4 x 10^{-7} m^2 s^{-1}), $\phi_{\partial_z T}(k_z)$ the vertical wavenumber k_z spectrum of the vertical gradient of temperature $\frac{\partial T}{\partial z}$, and k_o the lowest wavenumber of significant turbulence. The FP-07 measures vertical gradients of temperature well into the turbulent dissipation wavenumber regime.

Three transfer functions are applied to FP-07 sensor measurements to derive the temperature gradient spectrum; they are the analog-to-digital conversion H_{ADC}, amplification of the high-frequency component H_{Preamp}, and the response of the sensor to temperature fluctuations H_{FP07}, where H represents the transfer function. The analytical forms of the transfer functions H_{ADC} and H_{Preamp} are provided by manufacturers Cirrus Logic and Rockland Scientific, respectively.

The transfer function H_{FP07} is not known exactly and different findings have been reported (*Nash et al.* 1999; *Sommer et al.* 2013). We examine the effects of three double-pole transfer functions proposed by *Vachon and Lueck* (1984), *Gregg and Meagher* (1980), and *Sommer et al.* (2013) on our estimates of χ. The squared double-pole transfer function (H_{FP07}^2) is expressed as

$$H_{FP07}(f)^2 = \frac{1}{[1 + (2\pi f \tau)^2]^2}$$

where f is the frequency in Hz and τ is a constant characterizing the time in seconds of FP-07 sensor response to ambient temperature fluctuation. The time constant is suggested to vary with the flow speed relative to the sensor expressed as,

$$\tau = \tau_0 \left(\frac{U}{U_0}\right)^s$$

where τ_0 is a reference time constant, and U the flow speed relative to the sensor in m s^{-1} and U_0 = 1 m s^{-1}. The reference time τ_0 is 0.0064 s, 0.005 s, and 0.010 s, and the speed-dependence power law (s) is –0.5, –0.32, and 0 for the transfer functions suggested by *Vachon and Lueck* (1984), *Gregg and Meagher* (1980), and *Sommer et al.* (2013), respectively. At the typical EM-APEX float vertical profiling speed of 0.15 m s^{-1}, the time constant τ is 0.0155 s, 0.0092 s, and 0.010 s for the *Vachon and Lueck* (1984), *Gregg and Meagher* (1980), and *Sommer et al*. (2013) transfer functions, respectively. The latter two transfer functions are in very close agreement.

FP-07 sensors are mounted on the top end of EM-APEX floats, so measurements are taken only during ascending profiles to avoid potential wake effects. The FP-07 samples temperature at 120 Hz. Estimates of χ were computed from 4096 temperature data points over ~34-s duration, corresponding to ~5-m vertical bin for a typical EM-APEX float ascending speed of 0.15 m s^{-1}.

Computing χ from one timeseries of 34-s duration begins with the voltage measured by the FP-07 converted to temperature, then calibrated with the standard SBE41CP CTD sensor on the float (Fig. 3). The frequency spectrum of temperature is computed and converted to the vertical wavenumber spectrum assuming a frozen hypothesis using the average ascending float speed within the 34-s time interval (Fig. 3b). The vertical temperature gradient spectrum is computed as vertical wavenumber squared times the vertical wavenumber temperature spectrum (Fig. 3c). The vertical temperature gradient spectrum is then corrected by the above-mentioned three transfer functions. The H_{ADC} squared is white at low wavenumbers and rolls off beyond ~5 x 10^2 m^{-1}. The H_{Preamp} squared is white at the lowest wavenumbers, has a +2 spectral slope beyond ~10 m^{-1}, and rolls off at wavenumbers beyond that shown in Fig. 3e. Transfer functions proposed by *Sommer et al* (1984) and *Gregg and Meagher* (1980) are in close agreement, but that proposed by *Vachon and Lueck* (1984) rolls off at a frequency about 30% less (Fig. 3d).

The vertical temperature gradient spectra corrected by the three H_{FP07} transfer functions are in close agreement (Fig. 3e–f). Because of the low profiling speed, the roll-off spectral shape of the temperature gradient spectrum is fully resolved, implying that most turbulent temperature gradient variance is captured. The noise spectrum shows a spectral shape of k_z^2 at wavenumber greater than 10^3 m^{-1}.

Estimates of χ are computed by integrating the temperature gradient spectrum from k_z = 12 m^{-1} to an upper bound k_z beyond which the observed temperature gradient spectrum is smaller than the noise spectrum. The lower bound wavenumber 12 m^{-1} is determined after examining observed spectra. Estimated χ in this example is 4.9 x 10^{-9} K^2 s^{-1} using the FP-07 transfer function of *Vachon and Lueck* (1984) and 3.6 x 10^{-9} K^2 s^{-1} using those of *Gregg and Meagher* (1980) and *Sommer et al*. (2013). Estimates of χ derived from different transfer functions never differ by more than a factor of two. Note that because the full turbulent temperature gradient spectrum is resolved, estimates of χ are computed by integrating the observed temperature gradient spectrum over the turbulence range without the assumption of a model temperature gradient spectrum, as proposed by *Batchelor* (1959) or *Kraichnan* (1967). Observed temperature gradient spectra are in good agreement with the *Batchelor* (1959) temperature spectrum.

The turbulence diffusivity of temperature K_T can be computed following *Osborn and Cox* (1972) as

$$K_T = \frac{\chi}{2\langle \frac{dT}{dz} \rangle^2},$$

where $\langle \frac{dT}{dz} \rangle$ is the background temperature gradient. Assuming that the turbulence diffusivity of temperature K_T equals the turbulent diffusivity of buoyancy (e.g., *Moum and Nash*, 2009; *Alford and Pinkel*, 2000), defined as $K_\rho = \Gamma\varepsilon/N^2$, where ε is the turbulent kinetic energy dissipation rate, N the buoyancy frequency, and Γ the mixing efficiency assumed as the nominal value of 0.2, we can estimate ε as $\varepsilon = \frac{N^2\chi}{2\Gamma\langle \frac{dT}{dz} \rangle^2}$.

3. Results

3.1 Experimental observations

Twenty EM-APEX floats were deployed in the Sargasso Sea southeast of Cape Hatteras in 2011 as part of the ONR-funded Scalable Lateral Mixing and Coherent Turbulence Departmental Research Initiative (Fig. 4) (*Shcherbina et al*., 2015). All 20 EM-APEX floats measured temperature, salinity, pressure, and horizontal velocity components between the surface and typically 150-m depth, with some deeper profiles to ~250 m. Although the floats were at different locations, with separations up to 10 km, the units were programmed to rise nearly in synchronism. Extensive effort was made to synchronize the profiling floats. Simultaneous profiles eliminate differences caused by temporal versus spatial differences. Ten of the EM-APEX floats were equipped with dual FP-07 sensors. One of these χ-EM-APEX floats failed during the first deployment and was not used again in the experiment, and another was lost in the second deployment. Therefore, eight χ-EM-APEX floats provided turbulence measurements.

Floats were deployed in three settings (Fig. 4): Deployment (D1) was in a "weak energy" region during 3 – 10 June 2011 (4988 profiles), Deployment 2 (D2) was in a "strong front" during 13 – 16 June 2011 (2546 profiles), and Deployment 3 (D3) was conducted in a "strong current" during 17 – 20 June 2011 (2032 profiles) (Fig. 4). Floats were intended to be deployed in three concentric circles of 0.5 m, 1 km, and 2 km radii in the first two deployments, and of 1, 2, and 4 km radii in the third deployment, with roughly six floats on each circle. However, because of the oceanic horizontal shear, float arrays were not deployed in a perfectly concentric configuration.

During the 7-d mission of the first deployment, 20 EM-APEX floats were advected southeast about 20 km (Fig. 4). There was little dispersion of the float array. During the 3-d mission of the second deployment, the float array was strongly sheared in a front, while moved northeast for ~30 km. During the 3-d mission of the third deployment, the float array was advected northeast for 100 km.

3.2 Turbulence properties

The methods for computing χ, K_T, and ε are discussed in section 2.3. Because K_T and ε are derived quantities from measurements of χ and our purpose is to report the quality of turbulence measurements derived from FP-07 sensors on the EM-APEX floats, we will discuss only the quality of χ in the following analysis. The quality of χ will be assessed by three independent methods: (1) comparing the observed temperature gradient spectrum with the canonical form of the turbulent temperature gradient spectrum (*Batchelor*, 1959), (2) comparing estimates of χ obtained from different floats, and (3) comparing the statistics of χ estimates with the expectation for equilibrium turbulence.

In the following analysis, estimates of χ computed using the transfer function of *Gregg and Meagher* (1984) will be discussed. The ratio of estimates of χ computed from two FP-07 sensors has a mean ratio of 1.06, and the 95% confidence interval between 0.50 and 1.88. Estimates χ with the ratios between those obtained from two FP-07 sensors less a factor of two are averaged and discussed in the following analysis.

Observed temperature gradient spectra and their variance preserving spectra are compared with those of *Batchelor* (1959) at χ of 10^{-10}, 10^{-9}, 10^{-8}, 10^{-7}, and 10^{-6} $K^2\,s^{-1}$ (Fig. 5). Note that each observed temperature gradient spectrum is associated with distinct values of χ and ε . The Batchelor spectrum is computed for each corresponding observed spectrum with its associated χ and ε. These Batchelor spectra are averaged at different bins of χ and compared with the averaged observed spectra. Observed spectra agree well with Batchelor spectra near the roll-off wavenumbers, where most temperature gradient variance resides. They differ at low wavenumbers, where the temperature gradient variance is small and therefore does not contribute significantly to the estimate of χ. The noise level of our χ estimates is about 10^{-9} $K^2\,s^{-1}$, where the peak of the variance is closer to the noise. The noise is likely due to the amplified electronic noise in the float.

Vertical profiles of χ estimated from eight floats, averaged over each of three deployments, show similar vertical structures with their magnitudes typically within a factor of three from the means from all floats (Fig. 6). Estimates of χ obtained from different floats at different depths are strongly correlated with χ averaged over all floats with a correlation coefficient $R^2 = 0.94$, much higher than the 95% significance level of 0.07 (Fig. 7). The variation is less than a factor of two for χ greater than 3×10^{-9} $K^2\,s^{-1}$ and a factor of six for smaller χ, where the noise becomes significant (Fig. 5). The temperature signal is contaminated by electronic noise in the float. In a later version of the χ-EM-APEX system, the preamps are relocated outside the endcap to minimize the contamination by electronic noise from within the float.

The temporal variation of depth-averaged χ observed by different floats is similar most of time (Fig. 8). The greatest variability of depth-averaged χ , observed during 15–16 June, is presumably associated with a real oceanic signal of turbulence variability when the float array encountered a front (*Shcherbina et al*., 2015). At other times, the variability of the depth averaged χ of different floats is about a factor of two.

For statistically homogeneous isotropic turbulence, we expect ε and χ to have a lognormal distribution (*Yaglom*, 1960; *Gregg et al*., 1993; *Yamazaki*, 1990). The probability density function of χ estimates computed from all floats shows a nearly lognormal distribution, with a mean $\log_{10}(\chi)$ of –8.4 and a standard deviation of –0.9 (Fig. 9). The Quantile-Quantile (Q-Q) plot shows the quantile of observed $\log_{10}(\chi)$ vs. the standardized normal distribution (*Chambers et al.* 1983). The agreement is good for $\log_{10}(\chi)$ between –9.5 and –6.8, within ~1.2 standard deviation from the mean. *Yamazaki and Lueck* (1990) report that when turbulence is not statistically homogeneous, the observed turbulent kinetic energy dissipation rate ε might not exhibit a lognormal distribution. We suspect that the deviation of lognormal distribution at low χ is due to the measurement noise, and the deviation at high χ may be due to a violation of the assumptions of statistical homogeneity.

4. Discussion and conclusions

Our assessment of the quality of χ estimates is based on three independent methods. Estimates are reliable at values greater than order of 10^{-9} K^2 s^{-1}. Performance is at least comparable to that achieved in conventional microstructure free-fall profilers, such as χ estimates from Advanced Microstructure Profiler observations (*Lien et al*., 1995). Most importantly, because of the float's slow profiling speed, the roll-off regime of the turbulence gradient spectrum is captured. In comparison, free-fall microstructure profilers typically fall at a speed of 0.5–1 m s^{-1}, 3–7 times faster than the float's profiling speed, in order to capture turbulence shear variance measured from air-foil shear probes. Unfortunately, at this high speed, the roll-off wavenumber of the temperature gradient spectrum is often not captured by the FP-07 sensor.

The installation of FP-07 sensors on the eight EM-APEX floats used in the LatMix swarm was able to observe the small-scale temperature fluctuations associated with ocean turbulence. The observations conform to the expectations of the lognormal distribution of homogeneous turbulence at the intermediate levels of turbulence. Significant differences in turbulence temperature dissipate rates were calculated from floats across a front. This is expected in a region of spatial gradients in oceanic properties.

The performance of the χ system was adequate for this first application on the EM-APEX floats. There were some performance limitations. A concurrent installation of the RSI FP-07 and preamp/conditioning board on Seagliders by our colleagues Luc Rainville and Jason Gobat has a much lower noise level. This suggests that our design is contaminated by the amplified EM noise inside the float. The stainless steel metal stings also contributed corrosion noise that was observed on the Ag-AgCl electrodes near the end cap. These led to noise in the float's velocity measurements. Both of these effects have been reduced in the latest design. The thermistor preamps are now within the end cap, so that electronic noise within the float is not amplified and its contamination is minimized. Also, the stainless steel stings have been replaced with an all plastic holder for thermistor probes and preamps.

The need to recover the floats to extract data on the microSB card prevented the use of this design in other experiments. The latest firmware has been changed to provide log averaged spectral values. The amount of data to be transmitted over Iridium is expected to be about the same order as that for the CTD and velocity data.

Acknowledgements

Avery Snyder helped with the construction of χ–EM-APEX floats and supported the field operations during the LatMix experiment. We are grateful for the collaboration with Jason Gobat and Luc Rainville, especially in terms of future improvements for the implementation. We thank Steve Kahle for preparing Fig. 2. Financial support was provided by the Office of Naval Research Physical Oceanography Program under grants N00014-09-0194 and N00014-01-2184

References

Alford, M. H., and R. Pinkel (2000). Patterns of turbulent and double-diffusive phenomena: Observations from a rapid profiling micro-conductivity probe. *J. Phys. Oceanogr*., **30**, 833-854.

Batchelor, G. K. (1959). Small scale variation of convected quantities like temperature in turbulent fluid. Part 1: General discussion and the case of small conductivity. *J. Fluid. Mech*, **5**, 113-133.

Chambers, J. M., W. S. Cleveland, B. Kleiner, and P. A. Tukey (1983). Graphical methods for data analysis. Duxbury Press, 395pp.

Gregg, M.C., and T. B. Meagher (1980). The dynamic response of glass rod thermistors. *J. Geophys. Res.,* **85**, 2779-2786.

Gregg, M. C., H. E. Seim, and D. B. Percival (1993). Statistics of shear and turbulent dissipation profiles in random internal wave field. *J. Phys. Oceanogr*., **23**, 1777-1799.

Kraichnan, R. (1968). Small-scale structure of a scalar field convected by turbulence. *Phys. Fluids*,**11**, 945–953.

Lien, R. C., D. R. Caldwell, M. C. Gregg, and J. N. Moum (1995). Turbulence variability at the equator in the central Pacific at the beginning of the 1991-1993 El Nino. *J. Geophys. Res*., **100,** 6881-6898.

Moum, J. N., and J. D. Nash (2009). Mixing measurements on an Equatorial ocean mooring. *J. Atmos. Oceanic Technol.*, **26**, 317-335.

Nash, J. D., D. R. Caldwell, M. J. Zelman, and J. N. Moum (1999). A thermocouple probe for high-speed temperature measurement in the ocean. J. *Atmos. Oceanic Technol*., **16**, 1474-1482.

Osborn, T. R., and C. S. Cox (1972). Oceanic fine structure. *Geophys. Fluid Dyn.,* **3,** 321–345.

Sanford, T.B., R.G. Drever, J.H. Dunlap and E.A. D'Asaro (1982), Design, operation and performance of an Expendable Temperature and Velocity Profiler (XTVP). University of Washington, Applied Physics Laboratory Technical Report APL-UW 8110: 164 p.

Sanford, T. B., R. G. Drever and J. H. Dunlap (1985). An acoustic Doppler and electromagnetic velocity profiler. *J. Atmos. Oceanic Technol.,* **2**, 110-124.

Sanford, T.B., J.H. Dunlap, J.A. Carlson, D.C. Webb, and J.B. Girton (2005). Autonomous velocity and density profiler: EM-APEX. *Proceedings of the IEEE/OES Eighth Working Conference on Current Measurement Technology*, IEEE Cat No. 05CH37650, ISBN: 0-7803-8989-1, 152-156.

Shcherbina, A. Y., M. A. Sundermeyer, E. Kunze, E. D'Asaro, G. Badin, D. Birch, A.-M. E. G. Brunner-Suzuki, J. Callies, B. T. Kuebel Cervantes, M. Claret, B. Concannon, J. Early, R. Ferrari, L. Goodman, R. R. Harcourt, J. M. Klymak, C. M. Lee, M.-P. Lelong, M. D. Levine, R.-C. Lien, A. Mahadevan, J. C. McWilliams, M. J. Molemaker, S. Mukherjee, J. D. Nash, T. Özgökmen, S. D. Pierce, S. Ramachandran, R. M. Samelson, T. B. Sanford, R. K. Shearman, E. D. Skyllingstad, K. S. Smith, A. Tandon, J. R. Taylor, E. A. Terray, L. N. Thomas, and J. R. Ledwell (2015). The LatMix summer campaign: Submesoscale stirring in the upper ocean. *Bull. Amer. Meteor. Soc*., **96**, 1257–1279. doi: http://dx.doi.org/10.1175/BAMS-D-14-00015.1

Sommer, T., J. R. Carpenter, M. Schmid, R. G. Lueck, and F. Wuest (2013). Revisiting microstructure sensor responses with implications for double-diffusive fluxes. *J. Atmos. Ocean. Technol.,* **30**, 1907-1923.

Vachon, P., and R. Lueck (1984). A small combined temperature-conductivity probe. *Proc. 1984 STD Conf. and Workshop*, San Diego, California, Marine Technology Society San Diego Section and MTS Oceanic Instrumentation Committee, 126-131.

Yamazaki, H. A., and R. Lueck (1990). Why oceanic dissipation rates are not lognormal. *J. Phys. Oceanogr.*, **20**, 1907-1918.

Yamazaki, H. (1990). Breakage models: lognormality and intermittency. *J. Fluid Mech.*, **219**, 181-193.

Yaglom, A. M. (1966). On the influence of fluctuations in energy dissipation on the turbulence characteristics in the inertial internal. *Dokl. Akad. Nauk. SSSR*, **166**, 49-52.

Figure 1: Photos of EM-APEX float with electrode collar and rotation vanes (left) with dual fast-response temperature sensors FP-07 inside a guard (light green) and (right) a closer view of the FP-07 sensors, visible on black tips of metal shafts. Other components on the top of the float are the SBE41CP CTD in the center and the GPS/Iridium antenna.

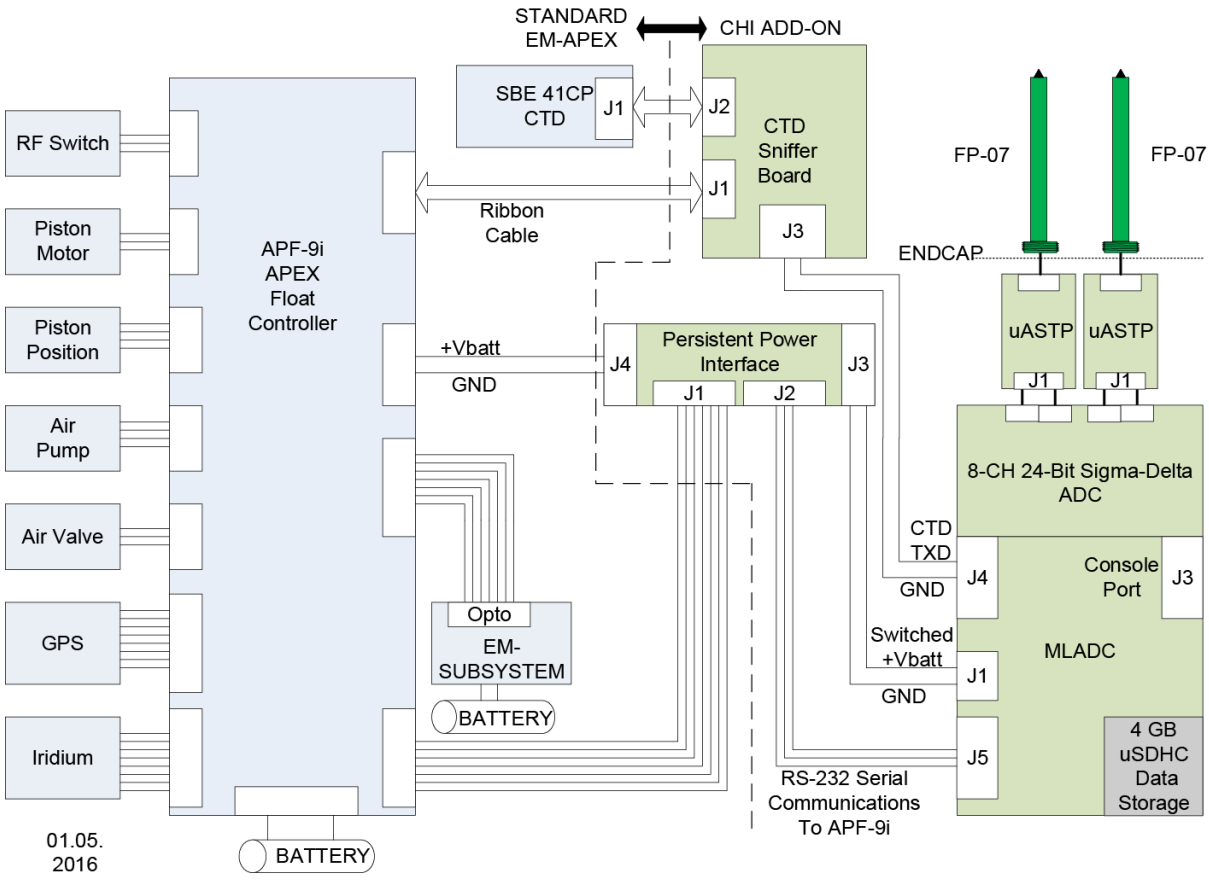

Figure 2: Block diagram of the χ-EM-APEX float. The left side of the dashed line shows the standard configuration for an EM-APEX float (grey). The APF9i APEX float controller runs the Sea-Bird CTD while using the air pump, air valve, and piston motor to control buoyancy. At the surface the APF9i uses a single antenna with an RF switch for GPS position information and Iridium communications. The right side of the dashed line shows the components added to make an χ-EM-APEX float (light green), including dual RSI FP-07 fast temperature probes (dark green), differential RSI pre-amps with a DC gain=x6 feeding into a 24-bit sigma-delta analog-to-digital converter and a dedicated χ-EM-APEX controller. The APF9i controls power to the χ system using the persistent power interface board. The χ controller on the MLADC board uses the CTD sniffer circuit board to intercept the data stream from the CTD to the APF-9i to gather rise and fall rate data. The resulting χ-EM-APEX data are stored on a MicroSD card. Reduced data are transmitted over the satellite link when on the surface, but the raw data are available only by removal of the storage card.

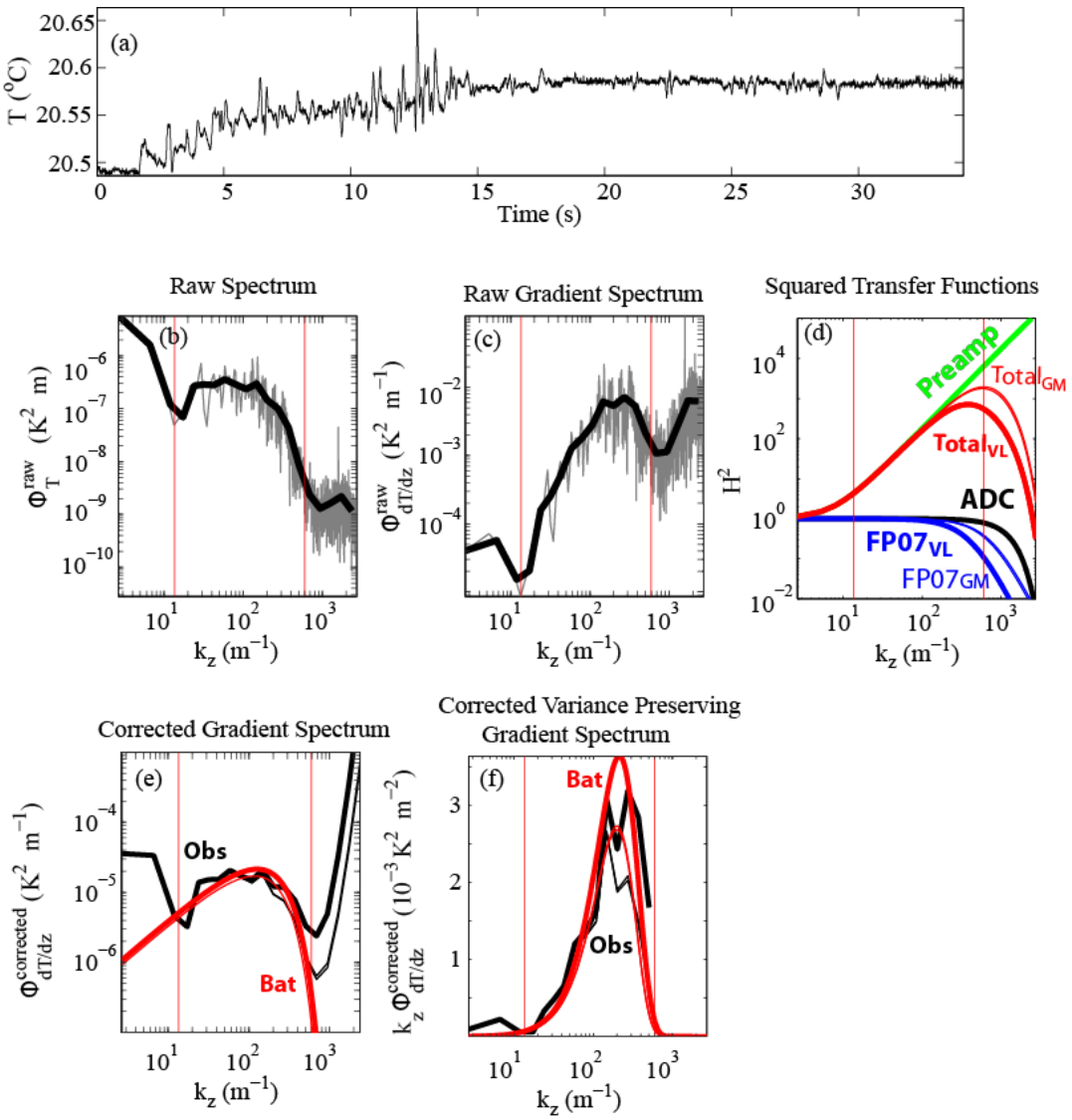

Figure 3: Examples of computing temperature variance dissipation rate χ from FP-07 measurements: (a) the time series of 35 s of temperature from one FP-07 sensor, (b) the observed raw temperature spectrum, (c) the observed raw spectrum of vertical gradient of temperature, (d) squared transfer functions of pre-amplifier (H_{Preamp}, green curve labeled as Preamp), analog-to-digital converter (H_{ADC}, ADC) (black curve labeled as ADC), FP-07 sensor ($H_{FP07,}$ thick blue curve labeled as $FP07_{VL}$ and thin blue curve labeled as $FP07_{GM}$), and the product of the above three transfer functions (thick red curve labeled as $Total_{VL}$ and thin red curve labeled as $Total_{GM}$), (e) observed temperature gradient spectrum corrected for transfer functions (thick and thin black curves labeled as Obs) and Batchelor temperature gradient spectrum (thick and thin red curve labeled as Bat), and (f) the variance preserving form of spectra shown in panel (e). The subscript 'VL' represents the use of FP-07 transfer functions proposed by *Vachon and Lueck* (1984). The subscript 'GM' represents the use of the transfer function suggested by *Gregg and Meagher* (1980), which is nearly identical to that of *Sommer et al.* (2013). Note that Batchelor spectra shown in panels (e) and (f) are computed using estimates of χ and ε obtained from observed

spectra. Thick and thin curves in panels (e) and (f) are computed using FP-07 transfer functions of *Vachon and Lueck* (1984) and *Gregg and Meagher* (1980), respectively.

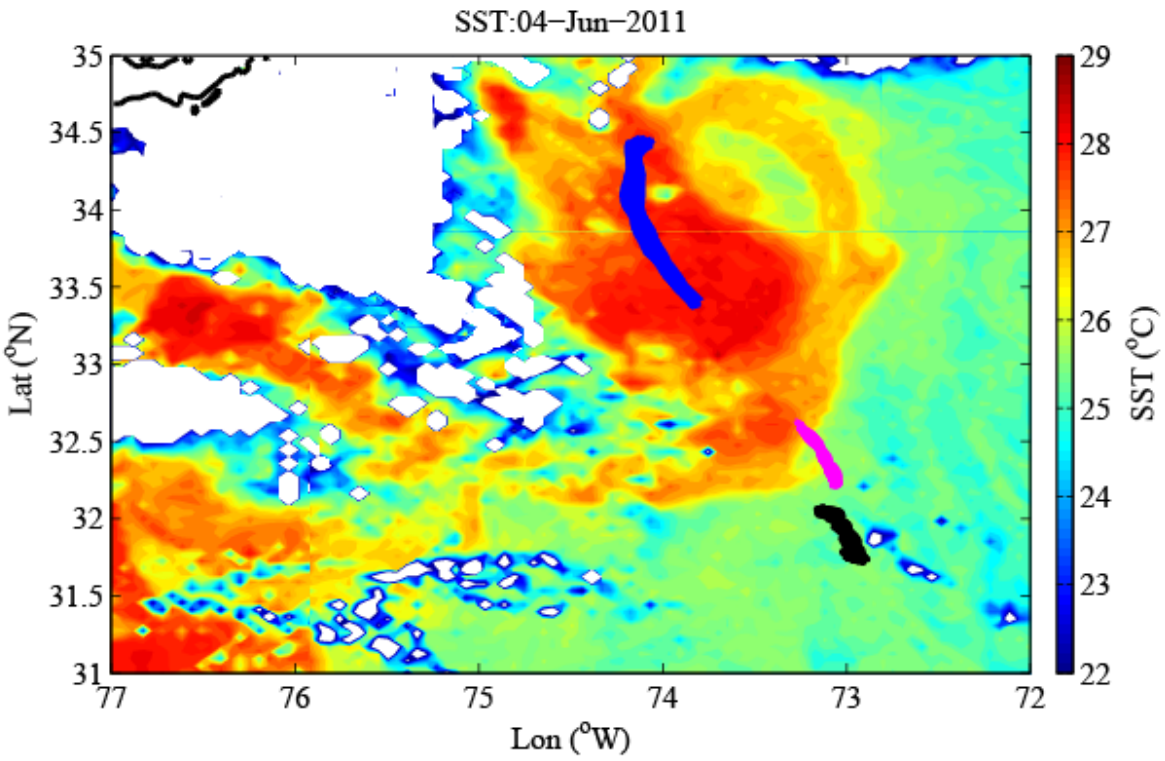

Figure 4: Float trajectories of three deployments during the LatMix experiment. Blue curves represent float trajectories on 6–10 June (D1), black curves on 13–16 June (D2), and pink curves on 17–20 June (D3). Background color shows the AVHRR image of SST on 4 June.

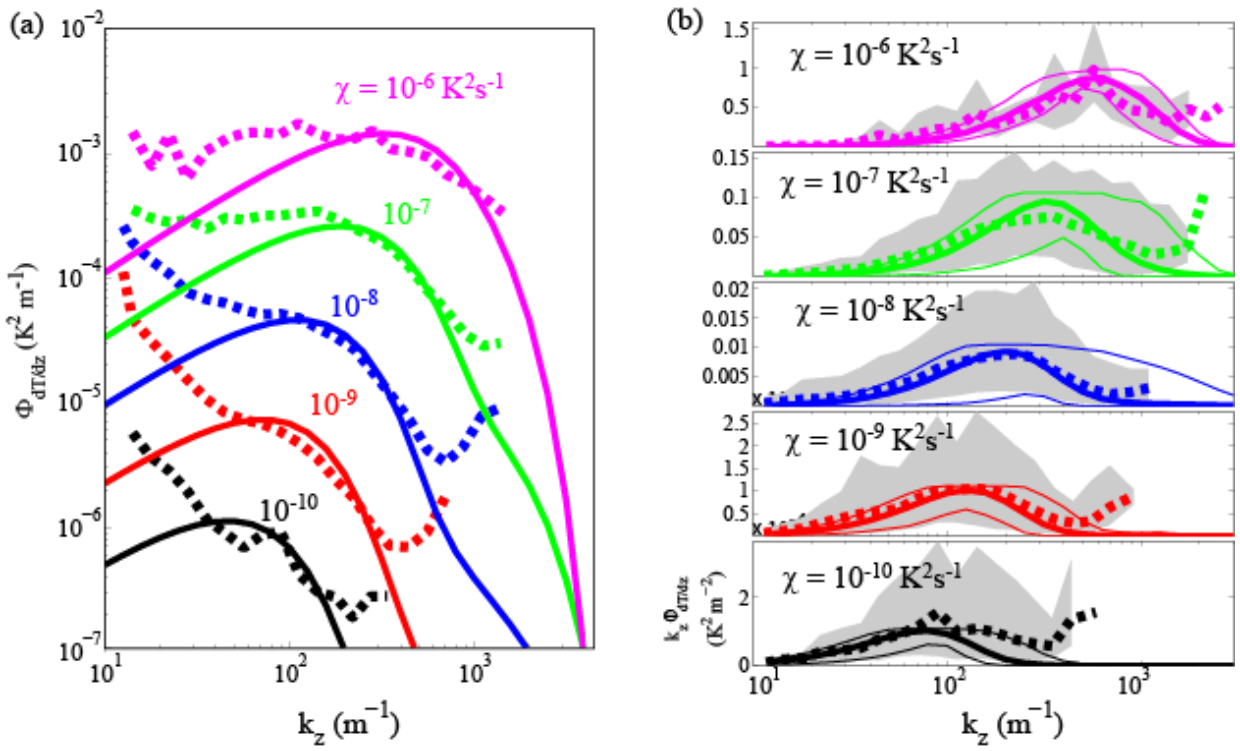

Fig. 5: (a) Comparison among observed temperature gradient spectra (dashed) with Batchelor spectra (solid) for χ of 10^{-10} – 10^{-6} $K^2\,s^{-1}$. (b) Similar to (a) but in variance preserving format. (b) Gray shadings represent 95% confidence interval of observed spectra, and thin curves represent 95% confidence interval of Batchelor spectra.

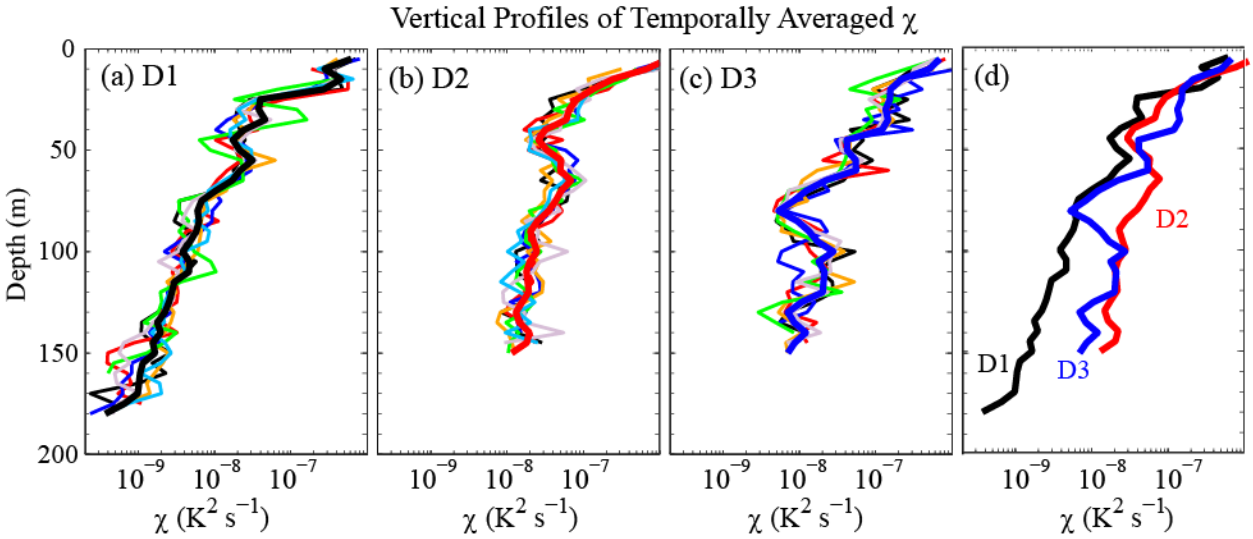

Figure 6. Vertical profiles of χ temporally averaged over three deployments of different floats (a–c) and averaged over all floats (d). In panels (a)–(c) different thin colored curves represent results from different floats, and the thick curves represent averages over all floats.

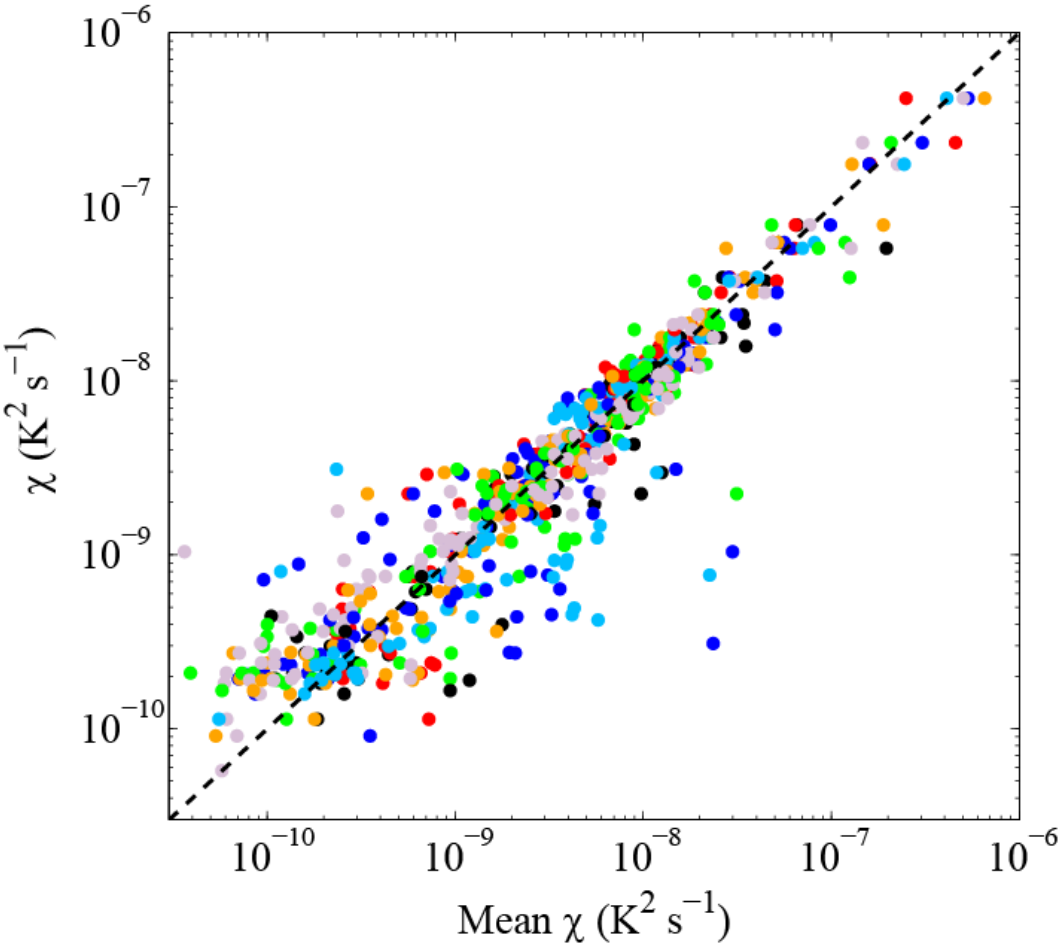

Fig. 7: Scatter plot of χ temporally averaged over each deployment period for different floats vs. χ temporally averaged over each deployment period and over all floats. Colors represent different floats.

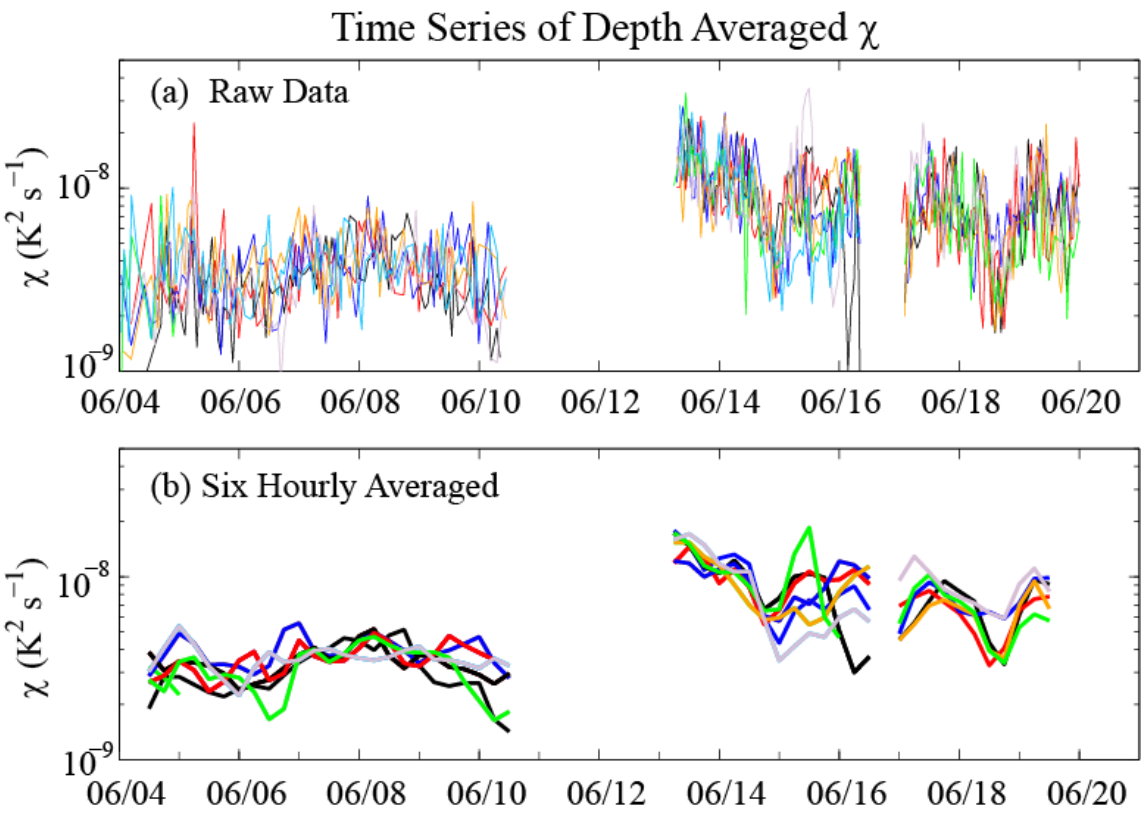

Fig. 8: (a) Time series of depth averaged χ from all floats, (b) six-hourly averaged values.

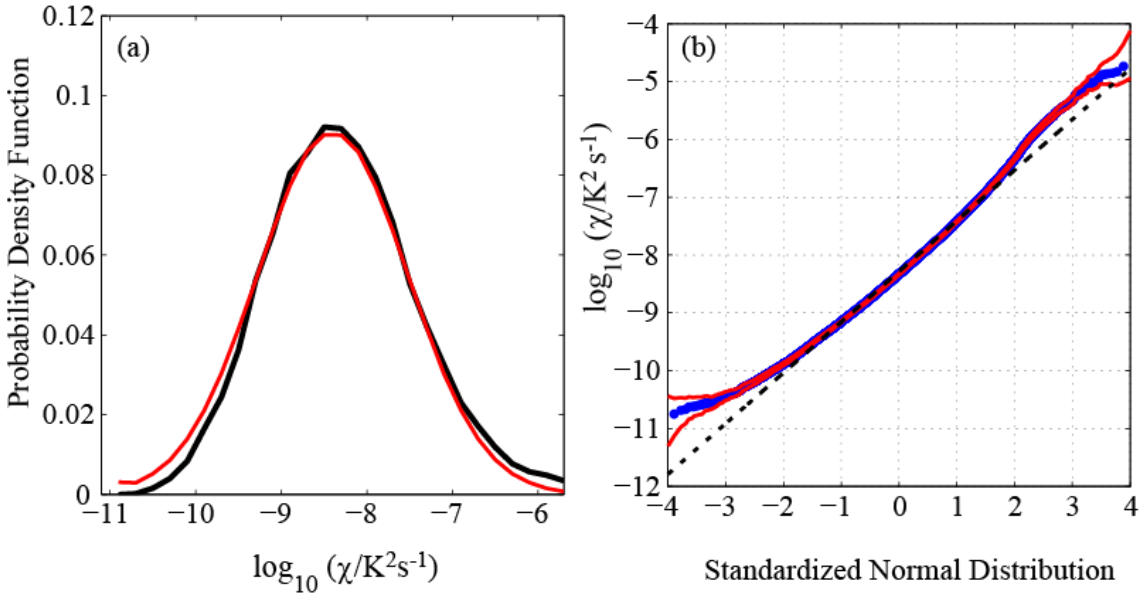

Fig. 9: (a) Probability density function of the ensemble of $\log_{10}(\chi)$ observations from all floats (black curve) compared with that expected from a theoretical normal distribution of the observed mean (–8.3) and standard deviation (0.9) (red curve). (b) Q-Q plot of $\log_{10}(\chi)$ vs. that of standardized normal distribution. The blue curve shows observed Q-Q structure. Red curves represent the 95% confidence interval assuming a normal distribution. The black dashed curve represents the theoretical normal distribution.

REPORT DOCUMENTATION PAGE

Form Approved
OMB No. 0704-0188

1. REPORT DATE *(DD-MM-YYYY)*	2. REPORT TYPE	3. DATES COVERED *(From - To)*
January 2016	Final Technical	01Jan2009 – 31Dec2015

4. TITLE AND SUBTITLE
Autonomous Microstructure EM-APEX Floats

5a. CONTRACT NUMBER

5b. GRANT NUMBER
N00014-09-1-0193

5c. PROGRAM ELEMENT NUMBER

6. AUTHOR(S)
Thomas B. Sanford
Ren-Chieh Lien
John Dunlap
James A. Carlson

5d. PROJECT NUMBER

5e. TASK NUMBER

5f. WORK UNIT NUMBER

7. PERFORMING ORGANIZATION NAME(S) AND ADDRESS(ES)
University of Washington – Applied Physics Laboratory
4333 Brooklyn Avenue NE
Seattle, WA 98105-6613

8. PERFORMING ORGANIZATION REPORT NUMBER

9. SPONSORING / MONITORING AGENCY NAME(S) AND ADDRESS(ES)
Office of Naval Research
One Liberty Center
875 North Randolph Street, Suite 1425
Arlington, VA 22203-1995

10. SPONSOR/MONITOR'S ACRONYM(S)
ONR

11. SPONSOR/MONITOR'S REPORT NUMBER(S)

12. DISTRIBUTION / AVAILABILITY STATEMENT

Distribution Statement A: Approved for public release; distribution is unlimited.

13. SUPPLEMENTARY NOTES

14. ABSTRACT

Fast responding FP-07 thermistors have been incorporated on profiling EM-APEX floats to measure microscale ocean temperature fluctuations produced by turbulence. In this implementation, the FP-07 thermistor generates an electrical signal corresponding to ocean temperature fluctuations, which is conditioned by an analog circuit board, and digitized and recorded to a custom data acquisition and storage board. The raw and processed temperature observations are stored on a microSD card. Results from eight microstructure EM-APEX floats deployed in the Sargasso Sea are presented here. The slow profiling speed of EM-APEX floats enables them to capture the higher wavenumber regime of microscale temperature variation. The quality of temperature variance dissipation rates χ estimated from microstructure EM-APEX floats is verified by their agreement with the Batchelor spectrum and by the close inter-float agreement of temporal and vertical variations measured by multiple floats. Estimates of χ from the profiling floats exhibit a lognormal distribution as expected for statistically homogeneous isotropic turbulence. Turbulence measurements derived from FP-07 sensors on autonomous profiling floats are of comparable quality to those on conventional free-fall microstructure profilers.

15. SUBJECT TERMS
profiling EM-APEX floats, FP-07 thermistors

16. SECURITY CLASSIFICATION OF:			17. LIMITATION OF ABSTRACT	18. NUMBER OF PAGES	19a. NAME OF RESPONSIBLE PERSON
a. REPORT	b. ABSTRACT	c. THIS PAGE			Tom Sanford
Unclassified	Unclassified	Unclassified	UU	20	19b. TELEPHONE NUMBER *(include area code)* (206) 543-1365